A Computationally Efficient MPC for Green Light Optimal Speed Advisory of Highly Automated Vehicles

Stephan Uebel[1], Steffen Kutter[1], Kevin Hipp[2] and Frank Schrödel[2]
[1]*Chair of Vehicle Mechatronics, Technische Universität Dresden, 01062 Dresden, Germany*
[2]*Development Center Chemnitz/Stollberg, IAV GmbH, 09366 Stollberg, Germany*

Keywords: Optimal Control, Sequential Quadratic Program, Velocity Control, Model Predictive Control, Green Light Optimal Speed Advisory, Highly Automated Driving, V2X.

Abstract: The current study introduces an approach for energy efficient longitudinal vehicle guidance. The key idea is to utilize a model predictive control (MPC) for the longitudinal vehicle dynamics which explicitly considers the current and the predicted states of multiple traffic lights ahead. Consequently, the vehicle can drive in urban situations much more energy efficient, which can be used to enlarge the range of electric vehicles or save fuel while additionally improving travel time. Modern traffic lights are equipped with transmitters that send information about their actual and upcoming system states. Additionally, traffic lights connected to a traffic control center can broadcast their future signal phases to vehicles many kilometers ahead. This information may be used to adapt the vehicle speed so that engine operation points are optimal and stops can be avoided. These kind of algorithms are referred to as green light optimal speed advisory. This work presents a novel online capable MPC approach that uses a sequential quadratic program to solve the respective optimal control problem. This approach is implemented in a framework introduced as well which allows driving tests in a real vehicle.

1 INTRODUCTION

The term green light optimal speed advisory (GLOSA) comprises all procedures for approaching traffic lights with vehicles in an optimal way by evaluating known or predicted information (traffic light phases). Corresponding assistance systems for passenger car drivers are well studied (Schuricht et al., 2011) and already available as prototypes today or are even in regular operation in trams (Gassel et al., 2012).

In order to overcome the computational burden of the underlying optimal control problem, typically simplified vehicle models and only few traffic light segments and phases (Erdmann, 2013) are taken into account or sub-optimal, not online capable methods like genetic algorithms (Seredynski et al., 2013) are utilized.

A major drawback of the implementation in form of a driver assistance system is the inclusion of the human driver as the overall controller in the system, since on the one hand there is an additional distraction from the primary driving task (safety) and on the other hand the driver's control performance (accuracy and speed) is poorer than technical systems.

With increasing vehicle automation the task of optimally choosing the vehicle velocity with respect to comfort, energy consumption and driving time is therefore handed over to the highly automated driving system (HAD). The HAD combines both lateral and longitudinal vehicle control with respect to the detected surrounding traffic situation and the planned path of the ego vehicle.

The current study focuses on optimizing the vehicle velocity in a HAD. Optimal velocity control has already been applied to conventional vehicles. For instance, an early implementation of real-time optimal velocity control using dynamic programming (DP) (Bellman, 1954) was presented by Porsche, called ACC InnoDrive (Radke, 2013). Other approaches using DP concentrate on controlling velocity on short-range trips, e.g. the distance between two traffic lights (Dib et al., 2011; Themann et al., 2014). Using DP for both, velocity control and gear shifting of conventional trucks, has been proposed in (Hellström et al., 2009; Hellström et al., 2010). Furthermore, DP is used for optimal velocity control of truck platoons (Bühler, 2013), but there, for the sake of compu-

Uebel, S., Kutter, S., Hipp, K. and Schrödel, F.
A Computationally Efficient MPC for Green Light Optimal Speed Advisory of Highly Automated Vehicles.
DOI: 10.5220/0007717304440451
In *Proceedings of the 5th International Conference on Vehicle Technology and Intelligent Transport Systems (VEHITS 2019)*, pages 444-451
ISBN: 978-989-758-374-2

tational efficiency, gear, internal combustion engine (ICE) on/off and travel time are removed from the state vector, and the engine model is reduced to a simple constant efficiency. Besides DP, other methods are examined for velocity control of conventional vehicles. For instance, quadratic programming (QP) (Boyd, 2004) has been proposed by (Gonsrang and Kasper, 2015). Early research calculating the optimal velocity of a conventional vehicle with Pontryagin's maximum principle (PMP) (Pontryagin et al., 1962) was done by (Schwarzkopf and Leipnik, 1977). A combination of QP and DP has been applied by (Murgovski et al., 2016) for optimal velocity control and gear selection for a platoon of conventional vehicles. Even the complex problem of computing the optimal velocity of hybrid electric vehicle is solved by the authors of (Uebel et al., 2018).

In contrast to the previous approaches mentioned, this paper presents a novel algorithm combining optimal longitudinal control and GLOSA for multiple traffic lights and phases into one, online capable control structure for a HAD. The algorithm uses a sequential quadratic program (SQP) (Mikosch et al., 2006, p. 529 ff.) to find the optimal solution. The close to optimal solution quality of this approach for a more complex problem is shown in (Uebel, 2018), by comparing the obtained results with the reference solution, calculated with DP on a high performance cluster at TU Dresden with over 8 months calculation time. In result with assuming no costs for changing gear, there is no deviation between the solutions but the computational effort can be reduced to a millionth. A case study for an implementation of the approach in a Volkswagen Golf passenger car is presented which shows the capability of the algorithm to compute the optimal trajectories for the velocity implemented at an online platform under real world driving conditions.

This paper is organized as follows. Section 2 introduces all model equations leading to the description of the discrete optimal control problem (OCP). Section 3 describes model abstractions that reduce the computation time for the SQP. Afterwards, it is shown how the SQP is used to solve the GLOSA problem. Finally, a case study is performed and discussed.

2 PROBLEM DESCRIPTION

In this section, the GLOSA problem is formulated. First a vehicle model is introduced which is used to derive an OCP afterwards.

2.1 Vehicle Model

The powertrain of the model includes an internal combustion engine (ICE) that converts chemical fuel energy to mechanical propulsion energy. The rotational speed of the ICE

$$\omega(v,g) = \frac{v}{\mathrm{r}}\gamma(g) \tag{1}$$

depends on the longitudinal vehicle velocity v, the dynamic rolling radius of the wheels r and the gear ratio $\gamma(g)$. Note, that g is not a control signal here because the gear yielding the lowest fuel consumption is selected at any instant (cf. 3.1).

The control signals are the ICE force $F_\mathrm{E} = T_\mathrm{E}/\mathrm{r}$ and the mechanical brake force F_B. They are gathered in the vector of inputs

$$\mathbf{u} = (F_\mathrm{E}, F_\mathrm{B}). \tag{2}$$

The force F_E is translated by the gearbox to a wheel force. The gearbox has an efficiency η_g that determines its dissipative force

$$F_{\mathrm{T,d}}(\mathbf{u}) = \begin{cases} F_\mathrm{E}(\eta_\mathrm{g}-1)/\eta_\mathrm{g}, & \text{for } F_\mathrm{E} \le 0 \\ F_\mathrm{E}(1-\eta_\mathrm{g}), & \text{for } F_\mathrm{E} > 0 \end{cases} \tag{3}$$

which counteracts the wheel force. The brake and the driving resistance due to inertia, air drag and road slope cause further counteracting forces. Accordingly, the balance of forces at the wheel is

$$\mathrm{m}v\frac{dv}{ds} + \mathrm{c_a}v^2 + c_\alpha + F_\mathrm{B} = (F_\mathrm{E} - F_{\mathrm{T,d}}(\mathbf{u}))\gamma(g), \quad \forall s \in [\mathrm{s_0}, \mathrm{s_f}], \tag{4}$$

where m is the vehicle mass, $\mathrm{c_a}$ is a constant for the air drag and c_α a slope-dependent disturbance that combines the rolling resistance and the force due to road gradient. The balance is formulated in a space coordinate s which denotes the travelled distance starting from an initial position $\mathrm{s_0}$ to a final position $\mathrm{s_f}$. The term vdv/ds in (4) derives directly from the time to space transformation

$$\frac{dv}{dt} = v\frac{dv}{ds}. \tag{5}$$

Note that, for brevity, the dependency on s is not displayed. All states and control signals and some coefficients in this paper depend on s. Constants that do not depend on s are displayed in upright letters. For instance in (4), $\mathrm{c_a}$ does not depend on s while c_α does.

It can be noticed that the state dynamics in (4) are nonlinear. A straightforward way to remove nonlinearity, without introducing approximations, is to perform a variable change, where kinetic energy

$$E_\mathrm{V} = \frac{1}{2}\mathrm{m}v^2 \tag{6}$$

is used as system state instead of longitudinal velocity. In space domain, the derivative of vehicle energy transforms into

$$\frac{\partial E_\mathrm{V}}{\partial s} = E'_\mathrm{V} = \frac{1}{2}\mathrm{m}\frac{dv^2}{ds} = \mathrm{m}v\frac{dv}{ds} = \mathrm{m}vv', \quad (7)$$

where the prime symbol ($'$) is used as a shorthand notation for the first derivative with respect to s. As a consequence of (7), (4) can be written as

$$\begin{aligned} &E'_\mathrm{V} = f_\mathrm{V}(\mathbf{u}, E_\mathrm{V}) = \\ &(F_\mathrm{E} - F_{\mathrm{T,d}}(\mathbf{u}))\gamma(g) - F_\mathrm{B} - 2\mathrm{c_a}E_\mathrm{V}/\mathrm{m} - c_\alpha \quad (8) \\ &\in \mathrm{m}[\mathrm{a_{min}}, \mathrm{a_{max}}], \end{aligned}$$

which gives the state differential equation of the kinetic energy f_V that is limited by the minimum acceleration $\mathrm{a_{min}}$ and the maximum acceleration $\mathrm{a_{max}}$, introduced to ensure driver comfort.

Since the problem is formulated in space coordinates, the travel time t becomes a system state. Its dynamics are expressed by

$$t' = 1/v = 1/\sqrt{2E_\mathrm{V}/\mathrm{m}} = f_\mathrm{t}(E_\mathrm{V}). \quad (9)$$

The system states are gathered in the complete state vector

$$\mathbf{x} = (\mathbf{x}_\mathrm{c}, \mathbf{x}_\mathrm{d}). \quad (10)$$

2.2 Problem Formulation

This section formulates the OCP in discrete space using the previously introduced model, where k is the discrete index for the position. The same symbols that were used in the continuous time representation, are used in this section to denote discrete signals.

The main objective is to minimize the monetary costs for a given route, subject to state and control constraints. The costs are expressed as the consumed fuel energy over the horizon multiplied by the respective price κ_E. The fuel energy is the product of the sample length $\Delta s(k)$ and the sum of F_E and the dissipative ICE force $F_{\mathrm{E,d}}(F_\mathrm{E}, \mathbf{x})$, which is provided by a lookup table.

The ensued OCP,

$$\begin{aligned} &\text{minimize } \mathcal{J}(\mathbf{u}(k), \mathbf{x}(k), k) \quad (11a) \\ &= \kappa_\mathrm{E} \sum_{k=1}^{N_\mathrm{k}} (F_\mathrm{E}(k) + F_{\mathrm{E,d}}(F_\mathrm{E}(k), \mathbf{x}(k))\gamma(g(k))\Delta s(k) \end{aligned}$$

subject to

$$\begin{aligned} &\mathbf{x}(k+1) = \mathbf{x}(k) + \mathbf{f}(\mathbf{u}(k), \mathbf{x}(k), k)\Delta s(k), \quad (11b) \\ &\mathbf{x}(1) = \mathbf{x}_0, \quad (11c) \\ &f_\mathrm{V}(k) \in \mathrm{m}[\mathrm{a_{min}}, \mathrm{a_{max}}], \quad (11d) \\ &\mathbf{x} \in [\mathbf{x}_{\min}(k), \mathbf{x}_{\max}(k)], \quad (11e) \\ &\mathbf{u} \in [\mathbf{u}_{\min}(\mathbf{x}(k)), \mathbf{u}_{\max}(\mathbf{x}(k))], \quad (11f) \end{aligned}$$

contains the function

$$\mathbf{f}(\mathbf{u}(k), \mathbf{x}(k), k) = (f_\mathrm{V}(k), f_\mathrm{t}(k)) \quad (12)$$

which combines the state dynamics of the states. The initial state conditions are given by the vectors $\mathbf{x}_0$ and the state space of the OCP (11) is bounded by lower ($\mathbf{x}_{\min}(k)$) and upper ($\mathbf{x}_{\max}(k)$) limits.

2.3 Velocity and Time Boundaries

An example for the boundaries on kinetic energy depitcs Figure 1, where the upper limit is obtained by

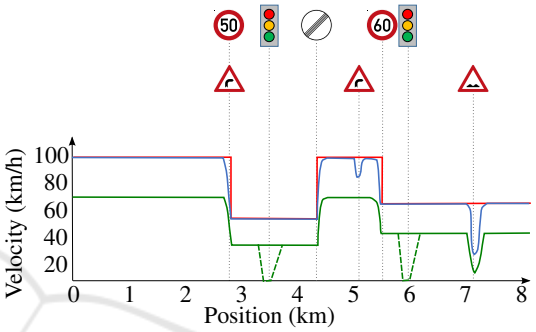

Figure 1: Boundaries to the velocity (kinetic energy). The red line represents the legal speed limit, while the blue line depicts limits due to a maximum cornering speed. The green line is the lower speed limit.

considering legal speed limits (red line). Additionally, demands on comfort (Bellem et al., 2016), (Reymond et al., 2001), (Scherer et al., 2015) as well as existing standards (International Organization for Standardization, 2009) limit the longitudinal and lateral acceleration, which lowers the maximum velocity (blue line). The lower bound on the velocity is obtained by subtracting a constant value from the upper speed limit (green trajectory). This value is influenced by the surrounding traffic, e.g. if the value is selected too high, the vehicle might be an obstacle. However, when approaching intersections and traffic lights lower velocities are accepted (green semicolon velocity) to enable a stop of the vehicle.

It can be understood that the time is bounded by the bounds on E_V. For example, the shortest time to a position can be derived following the upper limit on E_V (highest velocity). Additionally, the time is bounded by the timing of the traffic lights phases, which is illustrated in the upper plots of Figure 4 and 5 in the results section.

2.4 ACC and Stop-line Functions

Solving problem (11) purely in a MPC is not sufficient to implement a longitudinal velocity control

under real conditions (cf. Section 4). For example slower vehicles driving ahead on the same lane are neglected by the OCP. However, the solution of the OCP (11) can be used as a set velocity for a controller that works as a typical ACC when approaching a vehicle or can assure stopping at the stop line of a red traffic light.

Therefore, an algorithm solving (11) is utilized for the calculation of the optimal velocity with a long prediction horizon and explicit consideration of traffic lights. The computed target set is used for a shorter horizon by a lower level which contains an ACC and a stop-line approaching function.

A modular control design realizes both functions, which is a straightforward way of changing between different control modes. Following, three common modes are listed.

- Speed-based longitudinal dynamic control: The controller follows a given velocity which is obtained from the OCP algorithm. The controller structure corresponds to a conventional cruise control.
- Object-based longitudinal dynamic control: The controller uses sensor data to take vehicles driving ahead and other objects into account. The controller structure corresponds to a classic ACC.
- Trajectory-based longitudinal dynamic control: This mode realizes an accurate longitudinal dynamic trajectory tracking without imposing an additional dynamic on the system. In this controller mode, high requirements with regard to follow a given velocity trajectory (e.g. to brake at a stop line) must be realized in order to ensure driving comfort and safety to other road users.

In order to react to slower road participants driving ahead, the ACC reduces the desired speed, computed by the OCP algorithm. In detail, the distance to the vehicle ahead is controlled in an outer-control loop, which results in a new set speed for the vehicle, while the desired speed is controlled within the inner-control loop. In the current set up of the test vehicle, an acceleration instead of a velocity interface is used for the longitudinal guidance. Therefore, the chosen acceleration set point is transmitted to the acceleration controller, which computes the corespondent engine and brake torques.

Because of a higher update time the OCP algorithm cannot guarantee a stop at the precise position of the stop line. Due to this a trajectory-based longitudinal controller is used for stopping the vehicle. It activates if the velocity drops below a specific vehicle speed (e.g. 10 km/h) and uses an extra front camera and corresponding algorithms to determine the correct position of the stop line. This position is used to calculate a precise breaking trajectory.

3 GLOSA COMPUTATION

It is not straightforward to regard a set of time constraints which are imposed by the phases of a traffic light with the OCP formulated in the previous section. The reason is that the OCP formulation (11) allows only one value for the lower and one for the upper time boundary (cf. (11e)) at each instant (position) while several lower and upper boundaries are necessary to consider the phases of the traffic lights. Consequently, to find the optimal solution for the GLOSA problem the OCP has to be computed several time with different values for the time constraints at each computation. Consequently, in order to solve the GLOSA problem online, this section formulates the OCP as an SQP scheme, for which there are computationally efficient solvers.

3.1 Approximated Objective

Following, several steps are proposed to adapt the model in order to incorporate a fast solver[1] that decreases the computational demand, including abstraction of the engine transmission unit and a conservative QP modeling for an SQP scheme.

As stated before gear shifts are assumed to be instantaneous and the gears are optimized in advance, by preselecting gears that minimize fuel consumption when the ICE is propelling the vehicle. Thus, instead of investigating the fuel consumption map on the engine side, a corresponding fuel consumption map is generated for the engine transmission unit which provides the force $\tilde{F}_{\mathrm{E,W}}$ to the wheel. As there is a redundancy, in the sense that different gears may provide the same force-speed points, it is possible to chose optimal gears that minimize fuel consumption for each operating point. The obtained fuel consumption map is then approximated by the following analytic expression

$$\tilde{P}_{\mathrm{E}} = \zeta_0 + \sqrt{\tilde{E}_{\mathrm{V}}}(\zeta_1 + \zeta_2 \tilde{E}_{\mathrm{V}} + \zeta_3 \tilde{F}_{\mathrm{E,W}} + \zeta_4 \tilde{F}_{\mathrm{E,W}}^2 + \zeta_5 \tilde{E}_{\mathrm{V}}^2). \tag{13}$$

The over-line symbol tilde ($\{\tilde{\cdot}\}$) is used to denote approximated signals of the SQP.

The objective of the SQP is to minimize the monetary costs

[1] ECOS presented in (Domahidi et al., 2013) is used.

$$
\begin{aligned}
J(\tilde{t},\tilde{E}_\mathrm{V},\tilde{F}_\mathrm{E,W},\tilde{E}_\mathrm{S}) &= \kappa_\mathrm{E}\int_{s_0}^{s_\mathrm{f}}\frac{\tilde{P}_\mathrm{E}}{v}\mathrm{d}s \\
&= \kappa_\mathrm{S}(\tilde{E}_{\mathrm{S}0}-\tilde{E}_\mathrm{S}(s_\mathrm{f}))+\kappa_\mathrm{E}\zeta_0\int_{s_0}^{s_\mathrm{f}}\frac{1}{v}\mathrm{d}s+\kappa_\mathrm{E}\zeta_1\int_{s_0}^{s_\mathrm{f}}\mathrm{d}s \\
&+\kappa_\mathrm{E}\sqrt{\frac{m}{2}}\int_{s_0}^{s_\mathrm{f}}\left(\zeta_2\tilde{E}_\mathrm{V}+\zeta_3\tilde{F}_\mathrm{E,W}+\zeta_4\tilde{F}_\mathrm{E,W}^2+\zeta_5\tilde{E}_\mathrm{V}^2\right)\mathrm{d}s \\
&= \kappa_\mathrm{S}(\tilde{E}_{\mathrm{S}0}-\tilde{E}_\mathrm{S}(s_\mathrm{f}))+\kappa_\mathrm{E}\zeta_0(\tilde{t}(s_\mathrm{f})-\tilde{t}_0)+\kappa_\mathrm{E}\zeta_1(s_\mathrm{f}-s_0) \\
&+\kappa_\mathrm{E}\sqrt{\frac{m}{2}}\int_{s_0}^{s_\mathrm{f}}\left(\zeta_2\tilde{E}_\mathrm{V}+\zeta_3\tilde{F}_\mathrm{E,W}+\zeta_4\tilde{F}_\mathrm{E,W}^2+\zeta_5\tilde{E}_\mathrm{V}^2\right)\mathrm{d}s
\end{aligned}
\tag{14}
$$

which is a quadratic convex function. The terms including t_0 as well as the term multiplied by ζ_1 are constants that can be removed from the objective, without affecting the optimal solution. The objective can then be written in a discrete form, as discussed in Section 2.2.

3.2 Approximated Constraints

The maximum force that the engine-transmission unit can deliver is illustrated in Figure 2. It can be observed that the force limit is a highly nonlinear and partly discrete function. To remove the need for integer decisions, a piecewise nonlinear inner approximation is performed, of the form

$$
\tilde{F}_\mathrm{E,Wmax} = \min\begin{pmatrix}\zeta_{\mathrm{W},1}+\zeta_{\mathrm{W},2}\tilde{E}_\mathrm{V},\\ \zeta_{\mathrm{W},3},\\ \zeta_{\mathrm{W},4}+\zeta_{\mathrm{W},5}/\sqrt{\tilde{E}_\mathrm{V}}\end{pmatrix}. \tag{15}
$$

The inner approximation ensures that a solution obtained by solving the approximated problem is feasible also in the original problem. It can be observed in Figure 2 that the force limit, left of the peak point, is a concave function. A concave function can be approximated with a negligible error by expressing it as the minimum of sufficiently many affine pieces. Only two such pieces have been used here (the first two in (15)). Finally, the last, nonlinear piece in (15) is chosen to capture the power limit of the engine, as it is an alternative expression of an inverse speed relation.

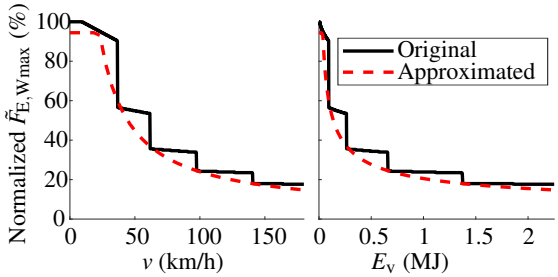

Figure 2: Approximated maximum force of the engine-transmission unit over velocity (left) and over kinetic energy (right) compared to the original model.

The nonlinear time dynamics,

$$
\tilde{t}' = 1/\sqrt{2\tilde{E}_\mathrm{V}/\mathrm{m}} \tag{16}
$$

cannot be expressed as a quadratic function and are therefore approximated using a reference kinetic energy, $\hat{\tilde{E}}_\mathrm{V}$, about which linearizations are performed; further discussed below.

The obtained optimization problem has now linear dynamics

$$
\tilde{E}_\mathrm{S}' = -\tilde{F}_\mathrm{S} \tag{17a}
$$

$$
\tilde{E}_\mathrm{V}' = \tilde{F}_\mathrm{E,W}-\tilde{F}_\mathrm{B}-2c_\mathrm{a}\tilde{E}_\mathrm{V}/\mathrm{m}-c_\alpha \tag{17b}
$$

$$
\tilde{t}' = 1/\sqrt{2\hat{\tilde{E}}_\mathrm{V}/\mathrm{m}} \tag{17c}
$$

but nonlinear and non-convex constraints, due to the nonlinear term $1/\sqrt{\tilde{E}_\mathrm{V}}$ in the force limits of the engine-transmission, (15). Due to the sign of the coefficients multiplying $1/\sqrt{\tilde{E}_\mathrm{V}}$, it can be observed that this term is convex. Therefore, linearizing it about the reference trajectory $\hat{\tilde{E}}_\mathrm{V}$,

$$
1/\sqrt{\tilde{E}_\mathrm{V}} \approx f_\mathrm{lin}(\tilde{E}_\mathrm{V},\hat{\tilde{E}}_\mathrm{V}) \tag{18}
$$

provides a convex inner approximation. This is the final ingredient for developing a computationally efficient SQP.

3.3 Approximated Problem Formulation

By defining the state and control vectors as

$$
\tilde{\mathbf{x}} = (\tilde{E}_\mathrm{V},\tilde{t}), \quad \tilde{\mathbf{u}} = (\tilde{F}_\mathrm{E,W},\tilde{F}_\mathrm{M,W},\tilde{F}_\mathrm{B}) \tag{19}
$$

and by discretizing with, e.g., zero-order hold, the resulting QP solved in each iteration of the SQP can be summarized as

$$
\text{minimize}\, J(\tilde{\mathbf{x}}(\tilde{k}),\tilde{\mathbf{u}}(\tilde{k}))+Q(\tilde{\mathbf{x}}(\tilde{k}),\tilde{\mathbf{u}}(\tilde{k})) \tag{20a}
$$

subject to

$$
\tilde{\mathbf{x}}(\tilde{k}+1) = \boldsymbol{A}(\tilde{k})\tilde{\mathbf{x}}(\tilde{k})+\boldsymbol{B}(\tilde{k})\tilde{\mathbf{u}}(\tilde{k})+\mathbf{w}(\tilde{k}) \tag{20b}
$$

$$
\boldsymbol{C}(\tilde{k})\tilde{\mathbf{x}}(\tilde{k})+\boldsymbol{D}(\tilde{k})\tilde{\mathbf{u}}(\tilde{k}) \le \mathbf{b}(\tilde{k}) \tag{20c}
$$

$$
\tilde{\mathbf{x}}(\tilde{k}) \in [\tilde{\mathbf{x}}_\mathrm{min}(\tilde{k}),\tilde{\mathbf{x}}_\mathrm{max}(\tilde{k})] \tag{20d}
$$

$$
\tilde{\mathbf{u}}(\tilde{k}) \in [\tilde{\mathbf{u}}_\mathrm{min}(\tilde{k}),\tilde{\mathbf{u}}_\mathrm{max}(\tilde{k})] \tag{20e}
$$

$$
\tilde{\mathbf{x}}(0) = \tilde{\mathbf{x}}_0, \quad \tilde{t}(N_\mathrm{k}) <= \tilde{t}_\mathrm{f} \tag{20f}
$$

$$
\tag{20g}
$$

where the matrices $\boldsymbol{A}$, $\boldsymbol{B}$, $\boldsymbol{C}$, $\boldsymbol{D}$ and the vectors $\mathbf{w}$, $\mathbf{b}$, $\tilde{\mathbf{x}}_\mathrm{min}$, $\tilde{\mathbf{x}}_\mathrm{max}$, can be found from eqs. (15) and (17). Note that these matrices and vectors depend on $\tilde{k}$ since the slope as well as the boundaries on $\tilde{E}_\mathrm{V}$ and the $\tilde{t}$ as well as the approximation of t' depend on the position. The distance between two samples $\tilde{k}$ might be

varying depending on the boundaries on $\tilde{E}_V$, i.e. at high velocities the sampling can be sparser.

The term Q in the objective is a standard term in the SQP framework that provides additional search direction towards the optimal solution that also minimizes the linearization error. It includes Hessian of the Lagrangian and Jacobian of the objective function, with respect to $\tilde{E}_V$. For further details, see (Mikosch et al., 2006). After each QP iteration, the trajectory about which the problem is linearized ($\hat{\tilde{E}}_V$) is updated by moving towards the direction of the current optimal solution. Thus, $\hat{\tilde{E}}_V$ is updated as

$$\hat{\tilde{E}}_V^{i+1} = \hat{\tilde{E}}_V^{i} + \xi(\tilde{E}_V^{i*} - \hat{\tilde{E}}_V^{i}) \tag{21}$$

where i is the current iteration, $*$ is the optimal solution in the current iteration and ξ is the step size that regulates the convergence rate. A high step size, $\xi = 1$, has been chosen for this problem. The initial trajectory $\hat{\tilde{E}}_V^1$ is selected as the mean between the upper and lower velocity boundaries.

4 CASE STUDY

This section presents a case study of the GLOSA approach. Before results for two different traffic light timings are shown, the test arrangement is presented.

4.1 Framework

The HAD framework depicted in Figure 3 consists of three layers which is similar to classic robotic solutions.

The first layer realizes the environment perception with the main focus on object detection and prediction as well as on lane detection and free space calculation. The second layer consist of decision making, including strategic, tactical and operational planing. The strategy module realizes route calculation and abstract mission planning. It derives prioritized missions and a route enhanced by abstract action requests. Therefore, it optimizes the whole route of the vehicle with respect to driving time, comfort and mission fulfillment.

The tactical module aims to generate optimal driving maneuver requests (e.g. lane change, lane keeping, parking) in order to follow the strategic route and actions. It continuously checks the driving state against the target state (e.g. target speed and target lane) and attempts to optimize the short term traveling behavior.

The operational module supplies atomic driving maneuvers such as lane keeping, lane change, etc. This lowest decision level knows the feasibility of each individual driving maneuver and tries to fulfill the requirements of the tactical level by using path planning algorithms. Below the decision layer, the trajectory planing and lateral and longitudinal vehicle dynamic controllers realize the detailed movement planing and tracing task in side the third layer.

4.2 Vehicle

The test vehicle which is used in the current study, is a VW Golf VII which is equipped with computation hardware (a dSPACE MicroAutoBox II and an industry PC).

4.3 Route

A test track near the airfield of the city of Dresden in Saxony/Germany was selected which is about 6.6 km long and equipped with four traffic lights. For future real driving tests these traffic lights are equipped with communication hardware in order to send the planned traffic light phases to the test vehicle.

4.4 Results

The longitudinal control of the approach is evaluated in two simulations: First, a simulation of the test track is performed where measured traffic light timings are used, to show the general capability of the algorithm to find the optimal speed through green phases of several traffic lights. For the second simulation the timing is changed, so the vehicle has to stop at the third traffic light.

The results of the two simulations are shown in the Figures 4 and 5, where the top plots shows the timing of the traffic light phases over the position. Additionally, the bound on the time derived from the minimum velocity is shown by the dotted line. It can be observed in both figures that following the minimum velocity would cause driving through a red light phase of the second traffic light. Due to this, the approach decreases the velocity yielding the one shown with the time trajectory depicted with a solid line in the upper plots.

The bottom plots show the associated velocity trajectories with solid lines, as well. The planned bounds on the velocity are shown with dotted lines. In order to avoid driving through red light, the minimum velocity has to be adapted which is done in the first half of the route. However, adaption is only allowed to about 60 % of the maximum velocity. Even with adaption of the velocity it is not possible to reach a

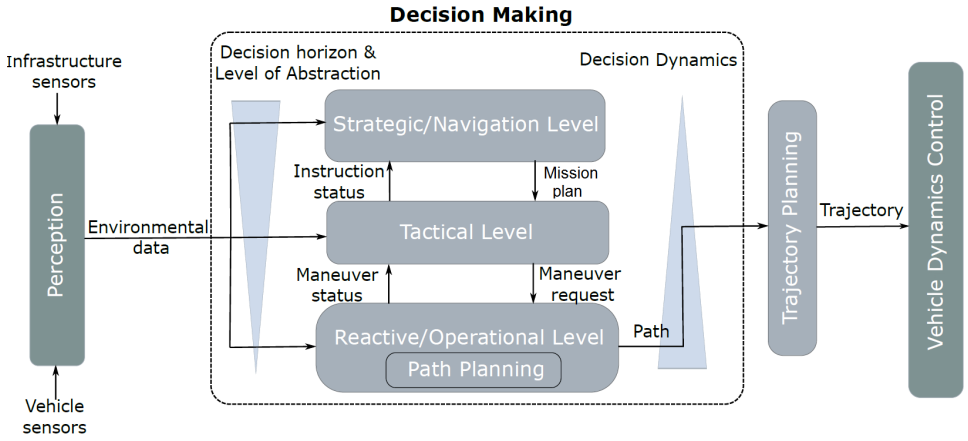

Figure 3: Functional Architecture for HAD System.

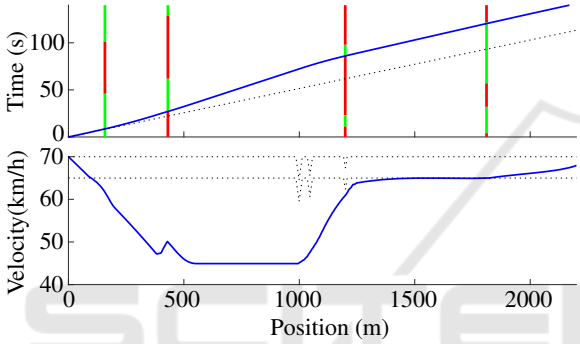

Figure 4: Results of the first simulation. The top plot shows the phase timing of the traffic lights and the time trajectory yielded by the algorithm, while the bottom plot depicts the associated velocity trajectory of the vehicle. The planned lower state bound for the velocity (lower dotted line) is violated at some instances in order to reach the green phase of the next traffic light.

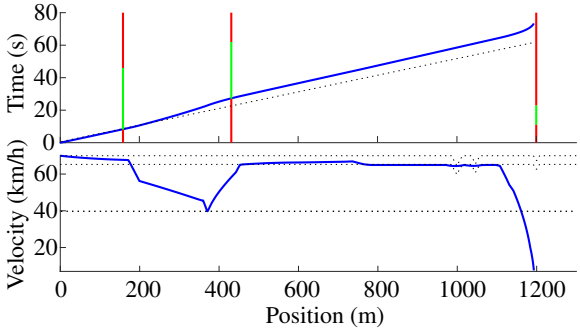

Figure 5: Results of the second simulation where a stop at the third traffic light is inevitable. In contrast to the first simulation, the vehicle accelerates to the minimum velocity before braking at the third traffic light.

green phase of the third traffic light in the second simulation shown in Figure 5. Consequently, the algorithm accelerates to the minimum velocity and brakes before the third traffic light. In order not be an obstacle for other road participants, the algorithm is configured to avoid a slow deceleration after the second traffic light which would be energy efficient. The major part of road users does not accept driving less than the minimum velocity shown in Figures 4 and 5 even when approaching a red light as we experienced in real world testing.

5 CONCLUSIONS

The simulations show that the introduced novel MPC algorithm for GLOSA which solves a set of OCPs using an SQP scheme is suitable for real driving tests. Performing these tests will be the next step. Therefore, the algorithm is already successfully implemented to the HAD framework presented in this paper where it performed with a turnaround time of about 0.2 s. The main challenge is to obtain a prediction of the traffic light phase timings with a sufficient horizon length since their signals are traffic-actuated.

ACKNOWLEDGEMENTS

The research shown here is related to the project initiative ”Syncronized Mobility 2023” and part of the projects ”REMAS”, ”SYNCAR” and ”HarmonizeDD” which are publicly funded by the European Union and the Federal Ministry of Transport and Digital Infrastructure in Germany. Additionally, the authors would like to thank The Center for Information Services and High Performance Computing (ZIH) at Technische Universität Dresden.

Supported by:

on the basis of a decision by the German Bundestag

REFERENCES

Bellem, H., Schönenberg, T., Krems, J. F., and Schrauf, M. (2016). Objective metrics of comfort: Developing a driving style for highly automated vehicles. *Transportation Research Part F: Traffic Psychology and Behaviour*, 41:45–54.

Bellman, R. (1954). The theory of dynamic programming. *Bulletin of the American Mathematical Society*, 60(6):503–515.

Boyd, S. (2004). *Convex optimization*. Cambridge University Press, Cambridge, U.K.

Bühler, L. (2013). Fuel-Efficient Platooning of Heavy Duty Vehicles through Road Topography Preview Information. Master's thesis, Automatic Control Laboratory - KTH Royal Institute of Technology, Stockholm, Sweden.

Dib, W., Serrao, L., and Sciarretta, A. (2011). Optimal control to minimize trip time and energy consumption in electric vehicles. In *2011 IEEE Vehicle Power and Propulsion Conference (VPPC)*, pages 1–8, Piscataway, New Jersey, USA. Institute of Electrical and Electronics Engineers (IEEE).

Domahidi, A., Chu, E., and Boyd, S. (2013). ECOS: An SOCP Solver for Embedded Systems. In *Proceedings European Control Conference*, pages 3071–3076, Zurich, Switzerland.

Erdmann, J. (2013). Combining adaptive junction control with simultaneous Green-Light-Optimal-Speed-Advisory. In *5th International Symposium on Wireless Vehicular Communications (WiVeC)*, pages 1–5.

Gassel, C., Matschek, T., and Krimmling, J. (2012). Cooperative Traffic Signals for Energy Efficient Driving in Tramway Systems. In Intelligent Transportation Society of America, editor, *19th ITS World Congress*.

Gonsrang, S. and Kasper, R. (2015). Optimization-based Energy Management System for Pure Electric Vehicles. In Bäker, B. and Morawietz, L., editors, *Energy efficient vehicles 2015: Visions, trends and solutions for energy efficient vehicle systems*, volume 5, pages 100–110. TUDpress, Dresden, Germany.

Hellström, E., Åslund, J., and Nielsen, L. (2010). Design of an efficient algorithm for fuel-optimal look-ahead control. *Control Engineering Practice*, 18(11):1318–1327.

Hellström, E., Ivarsson, M., Åslund, J., and Nielsen, L. (2009). Look-ahead control for heavy trucks to minimize trip time and fuel consumption. *Control Engineering Practice*, 17(2):245–254.

International Organization for Standardization (2009). ISO 22179:2009 - Intelligent transport systems - Full speed range adaptive cruise control (FSRA) systems - Performance requirements and test procedures: Performance requirements and test procedures.

Mikosch, T. V., Wright Stephen J, and Nocedal Jorge (2006). *Numerical Optimization*. Springer series in operations research Numerical optimization. Springer, New York, USA, 2 edition.

Murgovski, N., Egardt, B., and Nilsson, M. (2016). Cooperative energy management of automated vehicles. *Control Engineering Practice*, 57:84–98.

Pontryagin, L. S., Boltyanskii, V. G., Gamkrelidze, R. V., Mishchenko, E. F., and Pontrâgin, L. S. (1962). *The Mathematical Theory of Optimal Processes*. Interscience Publishers, New York, USA.

Radke, T. (2013). *Energieoptimale Längsführung von Kraftfahrzeugen durch den Einsatz vorausschauender Fahrstrategien*, volume 19 of *Karlsruher Schriftenreihe Fahrzeugsystemtechnik*. KIT Scientific Publishing, Karlsruhe and Hannover, Germany.

Reymond, G., Kemeny, A., Droulez, J., and Berthoz, A. (2001). Role of lateral acceleration in curve driving: driver model and experiments on a real vehicle and a driving simulator. *Human factors*, 43(3):483–495.

Scherer, S., Dettmann, A., Hartwich, F., Pech, T., Bullinger, A. C., and Wanielik, G. (2015). How the driver wants to be driven - Modelling driving styles in highly automated driving. Automatisiertes Fahren - Hype oder mehr? In Süd, T., editor, *7. Tagung Fahrerassistenz*, München.

Schuricht, P., Michler, O., and Baker, B. (2011). Efficiency-increasing driver assistance at signalized intersections using predictive traffic state estimation. In *14th International IEEE Conference on Intelligent Transportation Systems (ITSC), 2011*, pages 347–352, Washington, DC, USA.

Schwarzkopf, A. B. and Leipnik, R. B. (1977). Control of highway vehicles for minimum fuel consumption over varying terrain. *Transportation Research*, 11(4):279–286.

Seredynski, M., Dorronsoro, B., and Khadraoui, D. (2013). Comparison of Green Light Optimal Speed Advisory approaches. In *16th International IEEE Conference on Intelligent Transportation Systems (ITSC)*, pages 2187–2192, Piscataway, New Jersey, USA. Institute of Electrical and Electronics Engineers (IEEE).

Themann, P., Zlocki, A., and Eckstein, L. (2014). Energieeffiziente Fahrzeuglängsführung durch V2X-Kommunikation. *ATZ - Automobiltechnische Zeitschrift*, 116(7-8):62–67.

Uebel, S. (2018). Ein im Hybridfahrzeug einsetzbare Energiemanagementstrategie mit optimaler Längsführung. PhD thesis, Technische Universität Dresden, Dresden, Germany.

Uebel, S., Murgovski, N., Tempelhahn, C., and Baker, B. (2018). Optimal Energy Management and Velocity Control of Hybrid Electric Vehicles. *IEEE Transactions on Vehicular Technology*, 67(1):327–337.